RSC Advances

PAPER

View Article Online
View Journal | View Issue

Cite this: *RSC Adv.*, 2023, **13**, 7857

Regulation of polylactic acid using irradiation and preparation of PLA–SiO_2–ZnO melt-blown nonwovens for antibacterial and air filtration†

Yanlong Zhu,[a] Xiaoxia Gu,[a] Zhenfeng Dong,[a] Bin Wang, *[ab] Xu Jin,[a] Yankun Chen,[a] Meng Cui,[a] Rui Wang[a] and Xiuqin Zhang *[ab]

Received 28th December 2022
Accepted 24th February 2023

DOI: 10.1039/d2ra08274h

rsc.li/rsc-advances

Since the COVID-19 pandemic, polypropylene melt-blown nonwovens (MBs) have been widely used in disposable medical surgical masks and medical protective clothing, seriously threatening the environment. As a bio-based biodegradable polymer, polylactic acid (PLA) has attracted great attention in fabricating MBs. However, there are still issues with the undesirable spinnability of PLA and the limited filtration and antibacterial performance of PLA MBs. Herein, a high-efficiency, low-resistance, and antibacterial PLA filter is fabricated by melt-blown spinning and electret postprocessing technology. The irradiation technique is used to tune PLA chain structure, improving its spinnability. Further, silica (SiO_2) nanoparticles are added to enhance the charge storage stability of PLA MBs. With a constant airflow rate of 32 L min^{-1}, the PLA-based MBs exhibit a high particulate filtration efficiency of 94.8 ± 1.5%, an ultralow pressure drop of 14.1 ± 1.8 Pa, and an adequate bacterial filtration efficiency of 98 ± 1.2%, meeting the medical protective equipment standard. In addition, the zinc oxide (ZnO) masterbatches are doped into the blend and the antibacterial rate of PLA-based MBs against *Escherichia coli* and *Staphylococcus aureus* is higher than 99%. This successful preparation and modification method paves the way for the large-scale production of PLA MBs as promising candidates for high-efficacy and antibacterial filters.

Introduction

With the COVID-19 epidemic attacking the world, melt-blown nonwovens (MBs), as the core of masks, serve as the most effective solution to protect ourselves from the spread of droplets carrying the virus and aerogels in the air, becoming an indispensable material.[1,2] At present, the MBs on the market are almost all made of polypropylene (PP) that is non-degradable and difficult to recover, causing a great threat to the environment.[3] As a bio-based biodegradable polymer, polylactic acid (PLA) comes from renewable resources such as straw and starch in crops and is easy to recycle or decompose, having an advantage in disposable protective equipment.[4,5] However, PLA faces many problems in melt-blown spinning progress, *e.g.* poor spinnability, which significantly affects the filtration performance and mechanical properties of MBs.[6] Meanwhile, due to the absence of stable and effective electrets, limited charge storage capacity directly impairs the filtration performance of PLA MBs.[7] Moreover, the masks currently available on the market essentially lack antibacterial and antiviral properties, they can only intercept bacteria or viruses.[8,9] How to improve the melt-blown spinnability and further enhance the filtration performance and antibacterial ability of PLA MBs has become an important issue.

At present, there are some studies on regulating PLA melt-blown spinning parameters to improve the structure and filtration performance of MBs. Feng *et al.* optimized the filtration performance of PLA MBs by adjusting the collecting distance in melt-blown processing.[10] However, due to the melt index and crystallization rate of PLA can't fulfil the requirements of melt-blown processing, it is unable to radically improve the diameter and distribution of PLA MBs fiber. In other words, the filtration performance of PLA MBs still needs to be further improved.[11] The molecular chain structure of PLA is directly related to its melting index and crystallization rate.[12] Yang *et al.* adopted a laser-assisted melt-blown (LAMB) technique to manufacture PP MBs, which can substantially alter the viscosity of PP melt and enhance the filtration performance of MBs.[13] However, this method is too expensive for the industrial production of MBs. In contrast, irradiation technology is risk-free, environmentally friendly, and cost-effective. And it can be directly adapted to conventional processing operations

[a]*School of Materials Design & Engineering, Beijing Institute of Fashion Technology, Beijing 100029, China. E-mail: 20150010@bift.edu.cn; clyzxq@bift.edu.cn*

[b]*Beijing Key Laboratory of Clothing Materials R & D and Assessment, Beijing Engineering Research Center of Textile Nanofiber, Beijing Institute of Fashion Technology, Beijing 100029, China*

† Electronic supplementary information (ESI) available. See DOI: https://doi.org/10.1039/d2ra08274h

established in the industry for immediate mass production.[14,15] The irradiation technology mainly uses gamma ray and electron beam (EB) produced by cobalt-60 as the source of radiation.[16] As reported previously, the number average molecular weight of PLA decreased with the increase in irradiation dose, which is caused by two degradation mechanisms of PLA exposed to gamma rays in the air, namely, main chain breakage and hydrogen abstraction chain breakage.[17,18] Thus, the irradiation technology provides feasibility for increasing the melt index and improving the melt-blown spinnability of PLA.

Meanwhile, compared with the electret performance of traditional PP MBs, PLA MBs have some disadvantages, such as poor electret effect and fast surface charge attenuation, which directly impair the filtration performance of PLA MBs.[19] Many studies have shown that adding electret in MBs can effectively improve the filtration efficiency without increasing the pressure drop.[20] Electrets such as SiO_2,[21] titanium dioxide[22] and boehmite[23] have been widely used in air filters due to their advantages of charge storage capacity and stability. Correspondingly, Cheng *et al.* added SiO_2 to PLA MBs to obtain SiO_2/PLA composite MBs with excellent charge storage capacity and filtration performance.[24] Ding *et al.* fabricated a polyvinylidene fluoride (PVDF)/γ-glycidoxypropyl trimethoxysilane (GPS)@SiO_2 nanofiber membrane that exhibited a remarkable electret effect with a surface potential of 12.4 kV.[25] Yet, studies on the charge stability and time-dependent attenuation of PLA MBs by SiO_2 as electret are still limited, although there is of great significance for the long service life of PLA MBs as disposable protective materials.[26]

Additionally, in the era of the epidemic, the mask can effectively intercept bacteria and prevent human from inhaling bacteria in the air.[27] However, commercial PP or PLA filters lack antibacterial capability. According to reports, bacteria and viruses can survive in a general surgical mask for more than 4 days within the inner layer and 7 days on the outer layer.[28] Therefore, PLA MBs not only need to enhance high-efficiency and low-resistance filtration performance but also need to inactivate bacteria and viruses in time, inhibiting cross-infection caused by disposing of masks and medical protective clothing.[29] As a photocatalyst, zinc oxide (ZnO) is a common and efficient antibacterial agent, which has been safely and widely used in fibers, films, and other polymer matrixes.[30,31] The well-known mechanism is that ZnO may directly contact the cell walls of microorganisms and release reactive oxygen species through photocatalysis, resulting in the destruction of bacterial cell integrity.[32,33]

In this study, we report a facile strategy to fabricate high-efficiency and low-resistance and antibacterial PLA MBs *via* irradiation technology and melt-blown spinning processing. Firstly, it is inspired by the fact that irradiation can reduce the viscosity of PLA and further improve its spinnability.[13,14] We studied the effects of different irradiation doses on the molecular weight, viscosity and crystallinity of PLA. Then, by optimizing the weight ratio of irradiated PLA and pristine PLA, the composite MBs were successfully fabricated, and their structural properties, filtration performances and spinnability enhancement mechanism were investigated. Finally, PLA-based MBs with high filtration efficiency, excellent electret properties, and good antibacterial performance were fabricated by adding electret (SiO_2) and antibacterial agent (ZnO) to PLA melt. The effect of SiO_2 on the filtration performance and charge stability of MBs and the effect of ZnO on the antibacterial properties of MBs were further studied. PLA-based MBs prepared by this method exhibit important application potential in the field of disposable protective equipment.

Experimental section

Experimental raw materials

The polylactic acid (PLA, L9024) resin (Total Corbion Company, Thailand) had a viscosity-average molecular weight (Mv) of 8.26×10^4. The zinc oxide masterbatch (PLA content 83 wt%, ZnO particle diameter about 100 nm) product was purchased from Shanghai Aoling Textile New Material Co., Ltd, (SiO_2 nanoparticles diameter about 20 nm, China), and the SiO_2 electrostatic electret nanoparticles was purchased from Xinkui Polymer New Materials Co., Ltd, China.

Irradiation modification of PLA

Before irradiation, PLA was vacuum dried (24 h, 80 °C). The γ-radiation processing was performed by a γ-irradiator (Hongyi Sifang Radiation New Technology Co., Ltd, China), using a ^{60}Co irradiation source in the air at room temperature at a dose rate of 0.3 kGy h^{-1}. Samples being subjected to γ-doses of 50 and 100 kGy are named as PLAγ50 and PLAγ100, respectively.

Preparation of PLA melt-blown nonwovens

Initially, PLA, PLAγ50, PLAγ100, ZnO masterbatch and SiO_2 nanoparticles were dried in a vacuum oven at 80 °C for 24 h, and MBs were prepared by a melt-blown spinning machine produced by Beijing Institute of Fashion Technology. The schematic diagram of the melt-blown spinning process is shown in Fig. 1. In the experiment, the temperatures of the melt-blown spinning machine (Ts1, Ts2, Ts3, machine head, metering pump and spinneret) were set at 180, 185, 185, 195,

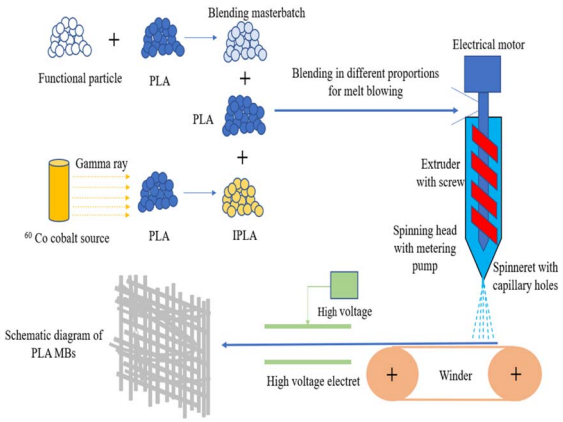

Fig. 1 Schematic diagram of irradiation and melt-blown spinning process.

195 and 195 °C, respectively. The materials were melted and extruded, hot-air drafted and self-bonded into web. The obtained MBs were named as PLA MBs, IPLA20 MBs (20 wt% PLAγ50 and 80 wt% pristine PLA), IPLA50 MBs (50 wt% PLAγ50 and 50 wt% pristine PLA), IPLA20-ZnO MBs (1 wt% ZnO masterbatch) and IPLA20-ZnO–SiO_2 MBs (1 wt% ZnO masterbatch and 1 wt% SiO_2 nanoparticles).

Characterization

The thermal property was investigated by means of differential scanning calorimetry (PerkinElmer DSC, Q2000, USA). The sample mass was about 6 mg with a continuous flow of nitrogen at 50 mL min^{-1}. Non-isothermal crystallization curve: sample was rapidly heated to 200 °C, equilibrated for 3 minutes to eliminate thermal history, cooled to 30 °C at the rate of 10 °C min^{-1} (cooling curve), and then heated to 200 °C (second heating). Isothermal crystallization curve: sample was quickly heated to 200 °C, then cooled for 30 minutes to 130 °C, and heated to 200 °C at a rate of 10°C min^{-1}. Graded crystallisation curve: the sample was heated to the first target temperature at a rate of 10 °C min^{-1}, held at a constant temperature for 3 minutes, then cooled to 30 °C and warmed to the next target temperature. The ramp-up and ramp-down steps were repeated, where the target temperatures were 200 °C, 173 °C, 169 °C, 165 °C, 161 °C and 200 °C, respectively. The Ubbelohde viscometer (model 3–0.47, Shanghai Shenshi Company, China) was used to test the viscosity of the sample. By gel permeation chromatography (GPC), a set of Waters 1525 GPC chromatographs and waters 2414 detector (USA) were used to detect the change of molecular weight and molecular weight distribution of the sample. Tensile testing of the MBs was carried out (provided by Shenzhen Wance Experimental Equipment Co., Ltd, TSE202A, China). The SEM image of the as-prepared MBs was photographed by JSM-7500F at an acceleration voltage of 5 kV. The fiber diameter was measured with Smile View software. A non-contact electric field compensation electrometer (FRASER 715, Fischer Electrostatic Elimination Equipment Co., Ltd, UK) was used to measure the surface electrostatic value of MBs after electret postprocessing. The porosity and pore size distribution of MBs were measured by the Auto Pore V9620 high-performance automatic mercury porosimeter (Merrittik Corp, USA). The pore size (r) was calculated using formula (1):[34]

$$r = \frac{-2\gamma \cos\theta}{P} \quad (1)$$

where P is the pressure used by the mercury porosimeter, γ is the surface tension of Hg (480 dynes cm^{-1}), and θ is the contact angle of mercury in the air (140°).

Air filtration performance test

An automatic filter material tester (TSI 3160 purchased from American TSI Inc) was used to test the filtration efficiency and pressure drop of MBs. The filtration efficiency and pressure drop of MBs to dioctyl phthalate (DOP) aerosols with different particle sizes were tested by controlling the airflow rate of 32 L min^{-1}, and the filtration efficiency (η) was calculated using formula (2):[20]

$$\eta = \left(1 - \frac{C_d}{C_u}\right) \times 100 \quad (2)$$

where C_u and C_d represent the concentrations of aerosol upstream and downstream, respectively. Calculate the average value of filtration efficiency by measuring the values of at least three samples. The quality factors (QF) were calculated using formula (3):[20]

$$QF = \left(\ln \frac{1}{(1-\eta)}\right) \Big/ \Delta P \quad (3)$$

where η (%) is the filtration efficiency along the particulates and ΔP is the pressure drop across the filter.

Bacterial filtration efficiency (BFE) of PLA-based MBs was evaluated and adapted from the standard YY 0469-2011 "Medical Surgical Mask".[35] Before the test, the sample was placed in an environment with temperature of 22 °C and relative humidity of 27% for pretreatment for 4 h. Bacterial suspension was prepared, and *Staphylococcus aureus* (ATCC6538) was inoculated into a proper amount of trypsin soybean broth, and cultured at 37 °C for 24 h. Then, the above culture was diluted with 1.5% peptone to a concentration of about 5×10^5 CFU mL^{-1}. The gas flow rate through the sampler was controlled at 28.3 L min^{-1}, the time of delivering bacterial suspension to the sprayer was set at 1 min, the air pressure and the running time of the sampler were set at 2 min, and the bacterial aerosol was collected on trypsin soybean agar. The agar plate was incubated at 37 °C for 48 h, and then the colony-forming units (positive holes) formed by bacterial aerosol particles were counted, and the obtained values were used to determine the average level of bacterial aerosol particles delivered to the test sample. Calculate the test results according to formula (4):[1]

$$BFE = \frac{C - T}{C} \times 100 \quad (4)$$

among them, C is the average value of positive quality control and T is the sum of test sample counts.

Antibacterial assays against *E. coli* and *S. aureus*

Antibacterial experiments were performed with two typical bacteria, Gram-negative *Escherichia coli* (ATCC 8099) and Gram-positive *Staphylococcus aureus* (ATCC 6538). Different strains of bacteria were cultured in soybean peptone broth at 37 °C for 24 h, and the broth was diluted 20 times with water. The concentration of the cultured bacterial solution was adjusted to 1×10^8 CFU mL^{-1}, which was used as the test bacterial solution. The control sample is white cotton cloth. Before the antibacterial test, all the samples were cut to 18×18 mm^2, weighed 0.4 g, and sterilized at 115 °C for 15 min, while retaining the characteristics of the samples. According to GB/T 20944.2 Textiles – Evaluation for Mntibacterial Mctivity—Part 2: Absorption Method, SCDLP liquid culture medium was added to the test bacteria solution, the bottle cap was closed tightly, and the bacteria were eluted by shaking 5 times (5 s each time)

at 37 °C for 18 h. The eluted 10-fold diluted solution is injected into a plate, and then about 15 mL of counting medium at 45 °C is added. After sealing, the plate is placed at room temperature, and after the medium solidifies, the plate is inverted and cultured at 37 °C for 18 h. According to the number of colonies (CFU) on the plate, use formula (5) to calculate the antibacterial rate:[1]

$$\text{Antibacterial rate } \% = \frac{B - A}{B} \times 100 \quad (5)$$

where B and A are the colony-forming units of the control group and the sample, respectively.

Results and discussion

Characterization of irradiated PLA

The mechanism of molecular weight (M_n) change of PLA caused by different doses of irradiation was studied by gel permeation chromatography. As shown in Fig. 2a and Table 1, the Mn of pristine PLA, PLAγ50 and PLAγ100 was 44 046, 32 137 and 24 491, respectively. This apparent drop in Mn with increasing doses of irradiation is due to the random chain scission rather than cross-linking.[36] Additionally, the literature pointed out that when the radiation dose is low, the large initial decrease in molecular weight is a consequence of long polymer backbone chains broken into chain segments. At higher radiation doses (>100 kGy), hydrogen abstraction becomes the key mechanism of radiation-induced chain scission.[34] The chain damage caused by this effect will inhibit the movement and crystallization of the PLA chain.[18] Viscosity will certainly decrease when PLA molecular weight drops, which is good for melt flow and curing moulding of PLA melt during melt-blown spinning processes.[38] As depicted in Fig. 2b, the viscosity of PLA considerably dropped from 0.926 to 0.688 and 0.543 Pa s^{-1}, respectively, as the irradiation dose rose from 0 to 50 and 100 kGy. The above shows that irradiation caused a decrease in the molecular weight and viscosity of PLA.

In order to explore the effect of radiation dose on the properties of PLA chain, we tested the graded crystallization of the sample by DSC, as shown in Fig. 2c. The DSC plots of PLA and PLAγ50 had only one melting peak at 178 and 173 °C, respectively. While PLAγ100 had two melting peaks and the melting temperatures further reduced to 171 and 167 °C. This evidence shows that the 100 kGy irradiation dose caused the decrease in PLA molecular weight and excessive chain scission. In contrast, PLAγ50 had a higher melting temperature and only one melting peak, and the chain scission induced by irradiation is moderate.[39]

DSC secondary heating curves of PLA and irradiated PLA are shown in Fig. 2d, and the corresponding thermal parameters are shown in Table 1. The glass transition temperature (T_g) of PLA, PLAγ50 and PLAγ100 was 59.6, 55.7 and 56.9 °C,

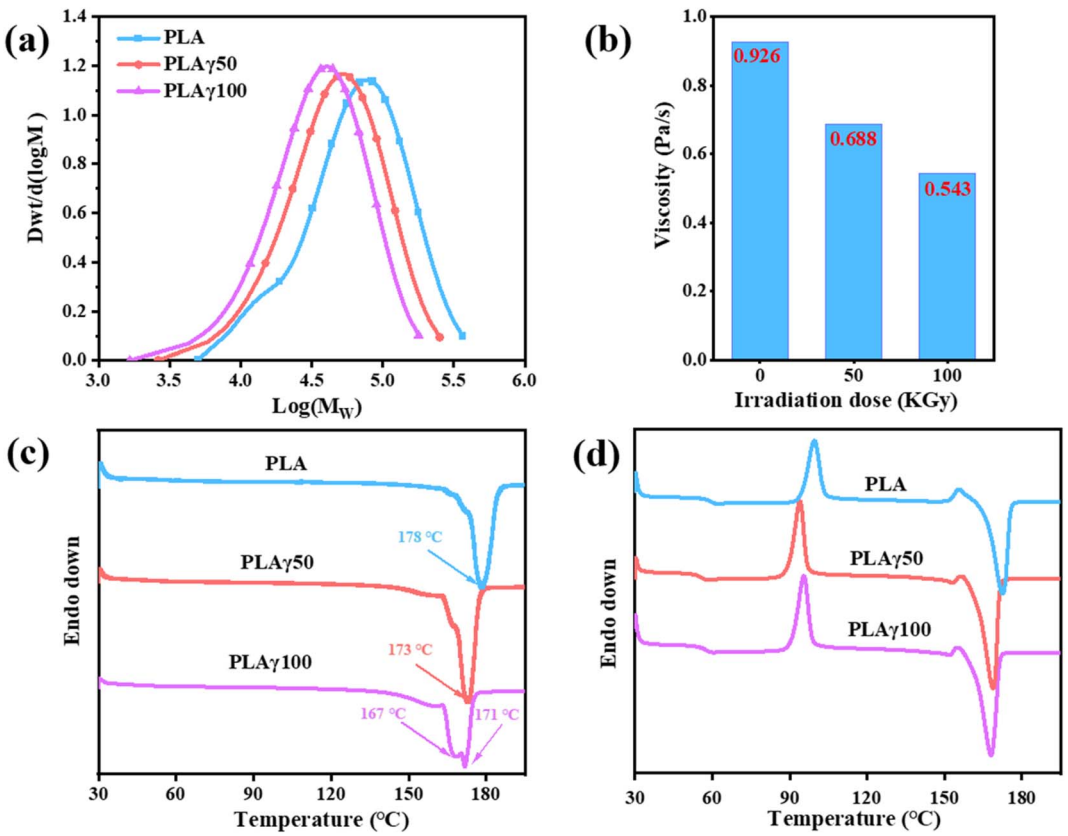

Fig. 2 Effect of irradiation on the structure of PLA. (a) GPC diagram, (b) viscosity diagram, (c) DSC grading crystallization diagram and (d) DSC secondary heating diagram.

Table 1 Molecular weight, viscosity and DSC data of PLA and irradiated PLA

	M_n	M_w	Viscosity	Cooling Xc_1 (%)	Second heating T_g (°C)	Second heating Xc_2 (%)	Isothermal Xc_3 (%)
PLA	44046	88972	0.926	2.5	59.6	16.9	36.9
PLAγ50	32173	61654	0.688	8.6	55.7	23.2	44.0
PLAγ100	24491	46092	0.543	7.2	56.9	21.1	42.7

respectively. The PLAγ50 showed the lowest T_g, which indicates that the chain of PLAγ50 could migrate at a lower temperature. The corresponding cold crystallization temperature was also the lowest (93.8 °C). The outstanding chain migration ability of PLAγ50 made the crystallinity up to 23.2%. This is due to the PLA chain broke into smaller fragments that migrate and crystallize at a lower temperature under γ-ray irradiation.[37] The cooling and isothermal crystallization curves of PLA, PLAγ50, and PLAγ100 are shown in Fig. S1 and S2.† Clearly, the crystallinity of PLAγ50 was the highest during the process of cooling and isothermal crystallization, and the maximum values are 8.5% and 44%, respectively. Thus, the lowest T_g and the highest crystallinity of PLAγ50 indicated outstanding chain migration capacity and crystallization ability. Due to excessive irradiation dose, the main chain of PLAγ100 was oxidized and scission.[40] Comparatively, the melting temperature (T_m) of PLA, PLAγ50 and PLAγ100 was 172, 168.8 and 168.1 °C, respectively, indicating that the PLAγ50 was more conducive to obtain sufficient melt fluidity at a lower processing temperature. Therefore, PLAγ50 is a good candidate for melt-blown spinning processing.

Morphology and structure analysis of irradiated PLA MBs

The geometric structure of MBs, including fiber diameter, porosity and pore size, had an important effect on the filtration performance.[41] Fig. 3a–c presents the SEM image and fiber diameter distribution of the PLA MBs, PLAγ50 MBs and PLAγ100 MBs. The fibers in PLA MBs are intertwined, with an average diameter of 7.36 μm (Fig. 3a). In addition, as the decrease of viscosity, the average fiber diameter of irradiated PLA MBs decreased obviously to 3.57 and 3.32 μm, which was consistent with the results of the previous literature.[42] Nevertheless, the fiber diameter distribution of PLAγ50 MBs was irregular, and some fibers are even broken. The fiber morphology and diameter distribution of PLAγ100 MBs were more undesirable, as shown in Fig. 3c. The possible reason is that the chain structures of PLAγ50 and PLAγ100 were destroyed by irradiation, and PLA with different lengths of chain can't be spun uniformly in the melt-blown spinning process, resulting in an uneven fiber diameter distribution.[18] Furthermore, when the fiber diameter of MBs is less than 2 μm, it is difficult to wind.

From the above, the irradiated PLA cannot be directly used alone for melt-blown spinning processing because its viscosity is too low and its chain is irregular. On the other hand, owing to pure PLA's high viscosity, it had poor melt fluidity and produced coarse-grained fibers, which were not conducive to air filtration performance. Therefore, in order to improve the spinnability of PLA, we designed to blend PLA with PLAγ50 in a certain proportion to prepare PLA MBs (named as IPLA MBs) with optimal fiber diameter and distribution.

Fig. 3d and e exhibits the morphology of IPLA20 MBs and IPLA50 MBs, respectively. The average fiber diameter of IPLA20 MBs reduced to 5.21 μm, without any obvious fracture or phase separation. The cause may be adding a proper amount of low viscosity PLAγ50 (20 wt%) can efficiently facilitate the melt flow of the blend, enhancing spinnability and lowering the fiber diameter of the resultant MBs.[43] Although the IPLA50 MBs have the smallest average fiber diameter of 3.51 μm, the number of fiber with a diameter of <2 μm accounts for up to 30%, significantly more than 0% of PLA MBs and 12% of IPLA20 MBs (Fig. 3e). IPLA 50 MBs have a poor spinning and winding state, which leads to uneven fiber diameter and distribution.

Compared to PLA MBs, the mechanical characteristics of IPLA20 MBs slightly declined. As shown in Fig. 3f, the breaking strength only dropped from 0.35 MPa to 0.32 MPa. However, the breaking strength of IPLA50 MBs is only 0.13 MPa. This further shows that the mechanical properties of MBs will reduce by adding irradiated PLA. But the mechanical decline of IPLA 20 MBs is relatively gentle, which meets the requirements of processing and application.

The pore size and distribution of PLA MBs and IPLA20 MBs are shown in Fig. 3g and h, respectively. Obviously, the porosity of PLA MBs was 79.9% and the average pore size was 20.1 μm. Due to the reduction in fiber diameter, the porosity of IPLA20 MBs increased to 89.81% and the average pore diameter increased to 42.7 μm. In fact, under the same processing condition, the smaller fiber diameter of the MBs, the higher porosity and the larger pore size of the MBs.[44] But the basis weight of MBs also affects the average pore diameter and the filtration performance further. In this work, we increased the basis weight to 35 g m^{-2} to adjust the average pore diameter when used to capture particulates in the air.

Functional modification of PLA MBs

In order to enhance the air filtration performance and antibacterial properties of PLA MBs, we introduced the functional modifiers ZnO (an antibacterial agent) and SiO_2 (an electret) into the blended melt of 80 wt% PLA and 20 wt% PLAγ50. The SEM images of IPLA20-ZnO MBs and IPLA20-ZnO–SiO_2 MBs are shown in Fig. 4a and b, respectively. Compared to IPLA20 MBs, fibers of IPLA20-ZnO MBs have a smooth surface, while IPLA20-ZnO–SiO_2 fibers have a slightly rougher surface with a few agglomerates. The fiber diameter of IPLA20-ZnO MBs and

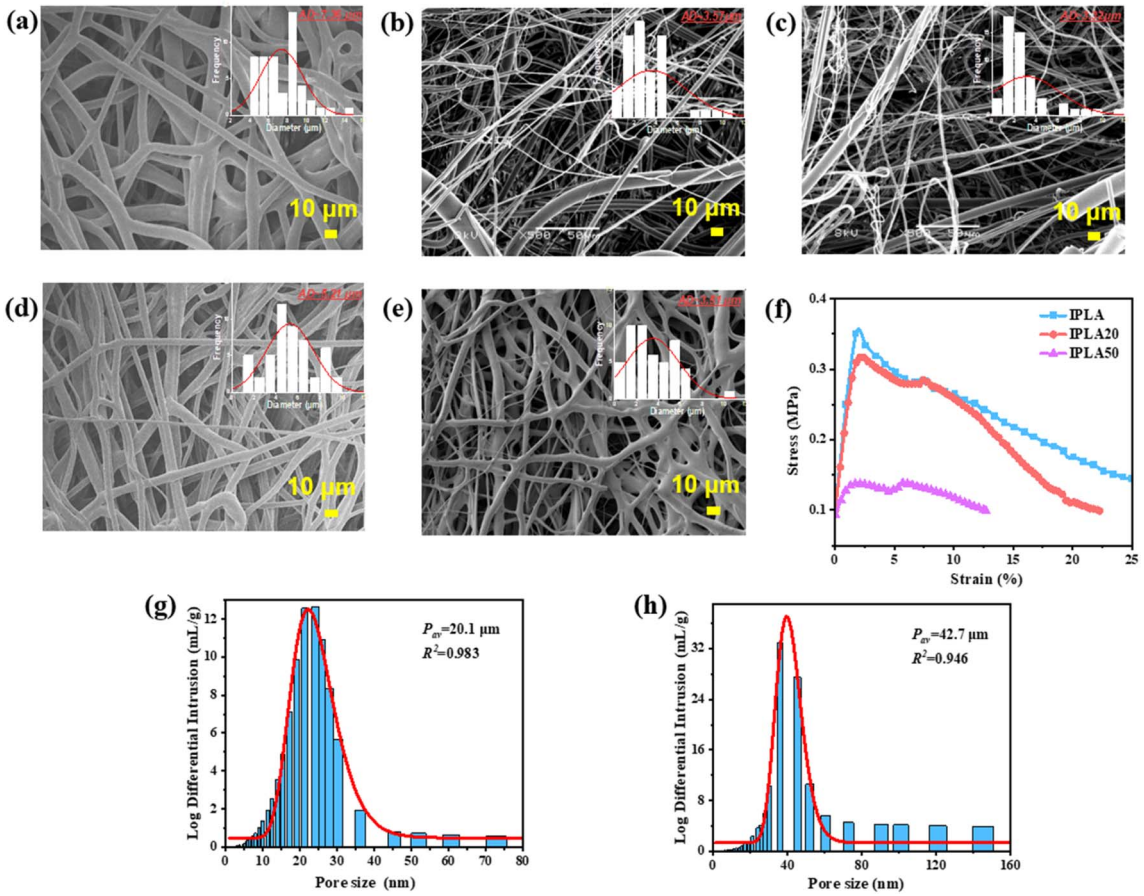

Fig. 3 Properties of irradiated PLA and PLA blend MBs. SEM images of (a) PLA MBs, (b) PLAγ50 MBs, (c) PLAγ100 MBs, (d) IPLA20 MBs and (e) IPLA50 MBs. (f) Stress–strain curve. Pore size and distributions of (g) PLA MBs and (h) IPLA20 MBs.

IPLA20-ZnO–SiO_2 MBs decreased to 5.13 μm and 4.95 μm, respectively. It was obvious that ZnO and SiO_2 could be added to PLA fibers to effectively reduce their diameter. According to Li *et al.*,[32] ZnO can accelerate heat absorption and promote the crystallization of PLA. Therefore, during melt-blown spinning process, the existence of ZnO and agglomerated SiO_2 was conducive to the curing of PLA fiber and reducing fiber diameter. The literature also noted that metal oxides could quicken heat absorption, reduce the viscosity of PLA, and accelerate the migration of PLA chain and melt flow.[45] This is equivalent to the application of irradiation technology to lower the viscosity of PLA, hence lowering the fiber diameter and enhancing the filtration performance of PLA MBs.

The average pore size of IPLA20 MBs, IPLA20-ZnO MBs and IPLA20-ZnO–SiO_2 MBs was 42.7, 38.1 and 27.3 μm, respectively (Fig. 4c and d). The porosity of three kinds of MBs was 89.81%, 88.13% and 74.69%, respectively. The decrease in the average pore size and porosity may be attributed to the presence of ZnO and SiO_2, leading to an increase in self-bonding spots between fibers in the MBs network during melt-blown spinning process. Low porosity and small pores created a long and challenging path for air penetration,[46] endowing MBs with high filtration efficiency. In addition, the higher number of self-bonding spots in the MBs leads to a tighter bond between the fibers and consequently to an increase in the stretching stress of MBs.

Electret technology is an important postprocessing in melt-blown spinning process. The electret will be charged under a high-voltage electrostatic field to store considerable charge and improve electrostatic adsorption between MBs and particulates.[47] Fig. 4e shows the changes in filtration efficiency and pressure drop of MBs before and after electret postprocessing at a fixed particulate size of 0.3 μm and an airflow rate of 32 L min^{-1}. Without electret postprocessing, the physical interception effect of MBs was mainly sieving interception, which was dependent on the structural properties of MBs themselves, such as fiber diameter, pore size and porosity.[42] As shown in Fig. 4e, the filtration efficiency of PLA MBs, IPLA20 MBs, IPLA20-ZnO MBs and IPLA20-ZnO–SiO_2 MBs without electret postprocessing was 36.5%, 42.6%, 49.3% and 50.1%, respectively. Compared with the PLA MBs, the filtration efficiency of the IPLA20 MBs has been improved, which is mainly due to the addition of the irradiation component which improved the spinnability of PLA and reduced the fiber diameter of MBs. Due to the incorporation of ZnO and SiO_2 decreased the fiber diameter, pore size and porosity of MBs, the filtration efficiency of IPLA20-ZnO MBs and IPLA20-ZnO–SiO_2 MBs was improved.

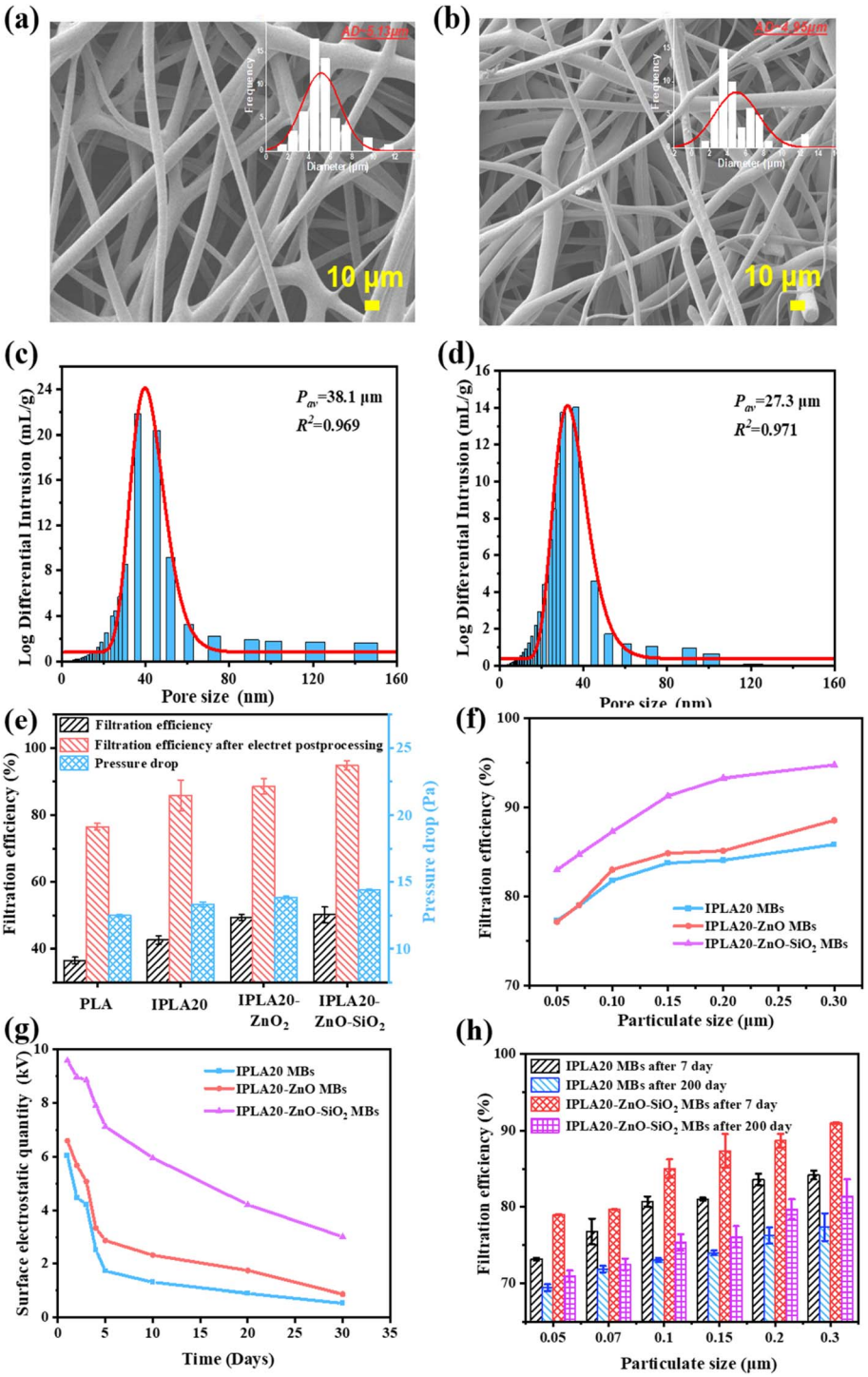

Fig. 4 Performance analysis of functionally modified MBs. SEM images of (a) IPLA20-ZnO MBs and (b) IPLA20-ZnO–SiO_2 MBs. Pore size distribution of (c) IPLA20-ZnO MBs and (d) IPLA20-ZnO–SiO_2 MBs. The filtration performance of MBs with (e) 0.3 μm particulate size and (f) different particulate sizes after electret postprocessing. (g) The change of surface static electret postprocessing with time. (h) The filtration efficiency of MBs with electret postprocessing for different particulate sizes after storage 7 days and 200 days.

After electret postprocessing, the electrostatic adsorption of the MBs was more obvious except for sieving interception, which was mainly due to the strong electrostatic force of charged MBs.[48] Therefore, as shown in Fig. 4e, the filtration efficiency of the MBs was greatly improved to 76.5%, 85.8%, 88.6% and 94.8%. With the addition of SiO_2 electret, the increasement of filtration efficiency of IPLA20-ZnO–SiO_2 MBs was much higher than that of PLA MBs, IPLA20 MBs, and IPLA20-ZnO MBs, which proved that SiO_2 electret has good charge storage capacity. In addition, the filtration efficiency of IPLA20-ZnO–SiO_2 MBs

reached 94.8% after electret postprocessing, totally meeting the filtration efficiency requirements of personal protective equipment.

Except for the nature of MBs, the filtration efficiency usually depends on the size of the target particulates.[48] Fig. 4f shows the filtration efficiency of MBs towards different particulate sizes after electret postprocessing. It is demonstrated that the filtration efficiency of IPLA20 MBs, IPLA20-ZnO and IPLA20-ZnO–SiO_2 MBs steadily increased as the particulate sizes rose, which is consistent with the trend in the literature.[11] As reported by Chmielewska *et al.*,[49] when the particulate size is smaller than 0.3 μm, the physical sieving effect is dominant, and the filtration efficiency increases as the particle size increases. At the same time, due to the pore size of IPLA20-ZnO–SiO_2 MBs is small, the filtration efficiency at different particulate sizes was higher than that of IPLA20 MBs. Furthermore, after electret postprocessing, the electrostatic adsorption effect of IPLA20-ZnO–SiO_2 MBs on capturing the fine particulates is stronger than that of IPLA20-ZnO MBs, due to the presence of electret SiO_2.

The variations in pressure drop for particulate filtering are shown in Fig. S3.† As can be seen, the pressure drop of MBs was maintained between 12 and 15 Pa and substantially smaller than that of the PP MBs, providing much better comfort.[50] Furthermore, after electret postprocessing, the pressure drop of MBs at different particulate sizes remains almost unchanged, due to the fact that electret postprocessing has no influence on the structure of MBs.[51] Quality factor (QF) can effectively reflect the comprehensive filtration performance of filters.[52] In Fig. S4,† the QF values of IPLA20 MBs and IPLA20-ZnO–SiO_2 MBs also increased with the increase in particulate size. And the maximum value of IPLA20-ZnO–SiO_2 MBs was 0.2 Pa^{-1}, higher than 0.15 Pa^{-1} of IPLA20 MBs, indicating that IPLA20-ZnO–SiO_2 MBs have excellent filtration performance due to the assistance of electret SiO_2.

The surface electrostatic value measured immediately after electret postprocessing reflected the ability of MBs to directly store charge. The amount of surface static electricity measured at different intervals reflected the material's ability to keep electrostatic charge, which was the ability to withstand the attenuation of electric quantity.[41] The change in surface electrostatic value of MBs with time is shown in Fig. 4g. The instant surface electrostatic value of IPLA20-ZnO–SiO_2 MBs was 9.58 kV, which is obviously greater than 6.04 kV of IPLA20 MBs and 6.59 kV of IPLA20-ZnO MBs. During the storage period of 30 days under darkness at room temperature, the surface electrostatic value of MBs showed a decreasing trend with time. The surface electrostatic value of IPLA20 MBs and IPLA20-ZnO MBs almost decreased to 0 kV, while that of IPLA20-ZnO–SiO_2 MBs still maintained above 3 kV, indicating that the addition of electret SiO_2 made the PLA MBs have excellent charge storage ability and resistance to charge decay. After placing of 7 days and 200 days, the filtration efficiency of IPLA20 MBs and IPLA20-ZnO–SiO_2 MBs with electret postprocessing is shown in Fig. 4h. The filtration efficiency of IPLA20-ZnO–SiO_2 MBs was stable after storage 200 days (81.4%) and was higher than that of IPLA20 MBs (77.4%). This is consistent with the result that the residual electrostatic charge level of IPLA20-ZnO–SiO_2 MBs is significantly higher than that of IPLA20 MBs, which further demonstrates that the prepared MBs had a long service life by incorporating SiO_2 electret.

When the MBs is used as a mask filter material, bacteria such as *E. coli* and *S. aureus* should be intercepted by MBs,[53] protecting humans from infection by the environment and others. Therefore, the bacterial filtration ability of MBs was also important for safety. The bacterial filtration test of IPLA20-ZnO–SiO_2 MBs is carried out according to the Chinese standard of YY0469-2011 (detailed in Air filtration performance test). The average BFE was 98.5%, which was higher than the requirement of BFE in Chinese standard, as well as the standard in European ASTM F2101-19 and American BS EN 14683: 2019.[54] Therefore, the IPLA20-ZnO–SiO_2 MBs as a mask filter material can effectively prevent pathogenic microorganisms, body fluids and particulate matter into human mouth and nose. It was of great significance to provide effective, safe, and green masks for human in the epidemic era of COVID-19.

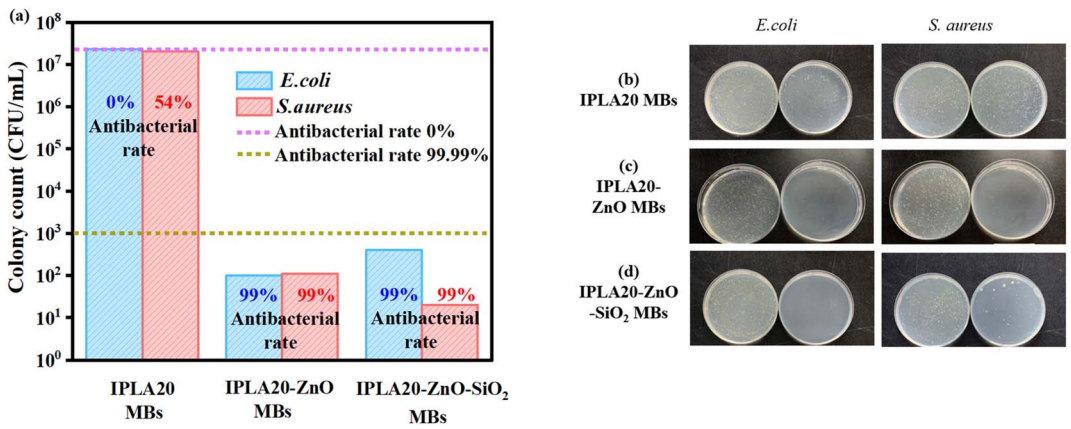

Fig. 5 (a) Colony number diagram and antibacterial rate of MBs after 18 hours of culture by *E. coli* and *S. aureus*, Colony status of (b) IPLA20 MBs, (c) IPLA20-ZnO MBs, and (d) IPLA20-ZnO–SiO_2 MBs.

Antibacterial property analysis of MBs

In order to measure the antibacterial properties of MBs, two typical bacteria, Gram-negative *E. coli* and Gram-positive *S. aureus* were used to contaminate MBs for 18 h. Fig. 5a show that after 18 hours of growth at a colony concentration of 2.0×10^5 CFU mL^{-1}, the number of viable *E. coli* and *S. aureus* in IPLA20 MBs grew to 2.3×10^7 CFU mL^{-1} and 2.0×10^7 CFU mL^{-1}, respectively. Compared with the viable count of the standard cloth, the antibacterial rate of IPLA20 MBs on *E. coli* and *S. aureus* was 0% and 54%, respectively. According to the standard of GB/T 20944.2 Textiles – Evaluation for Antibacterial Activity—Part 2: Absorption Method, IPLA20MBs has no antibacterial ability. The clear colonies in Fig. 5b further demonstrated that IPLA20 MBs do not meet the antibacterial standard that the antibacterial rate against *S. aureus* and *E. coli* should be greater than 99%. The colonies in IPLA20-ZnO MBs and IPLA20-ZnO–SiO_2 MBs are depicted in Fig. 5c and d, respectively. The colony count of *S. aureus* and *E. coli* dropped to 1.0×10^2 CFU mL^{-1}, and the antibacterial rate exceeded 99%. This shows that MBs containing ZnO have a significant antibacterial impact on *S. aureus* and *E. coli*. There are two explanations of the antibacterial mechanism of ZnO: (1) releasing Zn^{2+} ions that contact or enter cells to cause cell death, (2) generating reactive oxygenated species (ROS) and low-concentration H_2O_2 through photocatalysis, which leads to the denaturation and death of proteins, DNA, and fats in bacteria.[32,33] In general, adding ZnO to MBs is a simple and effective industrialized method for large-scale application in disposable masks, protective clothing and other medical equipment.

Conclusions

To sum up, we successfully designed an irradiation modified PLA with excellent spinnability of melt-blown spinning and a green IPLA20-ZnO–SiO_2 MBs that has high filtration efficiency, low pressure drop and antibacterial properties. Firstly, the chain structure of PLA was modified by irradiation technology, and irradiated PLA with low molecular weight, high crystallinity, and low viscosity was produced. Then, the IPLA20-ZnO–SiO_2 MBs was fabricated by adding electret SiO_2 and antibacterial agent ZnO into PLA melt during the melt-blowing spinning process. Finally, the IPLA20-ZnO–SiO_2 MBs possessed high filtration efficiency up to 94.8%, low pressure drop of 14 Pa and satisfied QF value of 0.2 Pa^{-1} at an airflow rate of 32 L min^{-1} and particulate size of 0.3 μm. Meanwhile, the bacterial filtration efficiency was higher than 99%. Furthermore, this material exhibited excellent charge storage ability and stability and maintained outstanding filtration performance even after storing for 200 days, ensuring its long-term storage and service. In addition, the antibacterial rate of IPLA20-ZnO–SiO_2 MBs against *S. aureus* and *E. coli* reached up to 99%, respectively. In general, we anticipate that the PLA-based melt-blown nonwovens will have tremendous potential for the application of disposable medical surgical masks and medical protective clothing.

Author contributions

The manuscript was written through contributions of all authors. All authors have given approval to the final version of the manuscript.

Conflicts of interest

The authors declare no conflict of interest.

Acknowledgements

This work was supported by National Natural Science Foundation of China (52173027, 51929301, 52103069), Beijing Municipal Education Commission-Beijing Natural Science Foundation (22JB0025), Beijing Scholars Foundation (RCQJ20303), and Inter School Cooperation Program for Innovation and Entrepreneurship Training of College Students in Beijing (202298026).

Notes and references

1 P. Ekabutr, P. Chuysinuan, S. Suksamrarn, W. Sukhumsirichart, P. Hongmanee and P. Supaphol, *Polym. Bull.*, 2019, **76**, 1985–2004.
2 C. Tsutsumi Arai, Y. Iwamiya, R. Hoshino, C. Terada Ito, S. Sejima, K. Akutsu Suyama, M. Shibayama, Z. Hiroi, R. Tokuyama Toda, R. Iwamiya, K. Ijichi, T. Chiba and K. Satomura, *Int. J. Environ. Res. Public Health*, 2022, **19**, 3639–3649.
3 L. Shao, Y. C. Chang, C. Hao, M. e. Fei, B. Zhao, B. J. Bliss and J. Zhang, *Green Chem.*, 2022, **24**, 8716–8724.
4 Y. Qi, H. L. Ma, Z. H. Du, B. Yang, J. Wu, R. Wang and X. Q. Zhang, *ACS Omega*, 2019, **4**, 21439–21445.
5 X. X. Chen, J. C. Yu, K. Chen, P. Ji, X. L. Chen and Z. J. Pan, *Chin. J. Polym. Sci.*, 2022, **40**, 1242–1251.
6 H. Sun, S. Peng, M. Wang, F. Zhu, G. Bhat and B. Yu, *J. Eng. Fibers Fabr.*, 2020, **15**, 1–13.
7 H. Xiao, J. Gui, G. Chen and C. Xiao, *J. Appl. Polym. Sci.*, 2015, **132**, 42807–42812.
8 X. Y. D. Soo, S. Wang, C. C. J. Yeo, J. Li, X. P. Ni, L. Jiang, K. Xue, Z. Li, X. Fei and Q. Zhu, *Sci. Total Environ.*, 2022, **807**, 151084–151093.
9 E. Vaňková, P. Kašparová, J. Khun, A. Machková, J. Julák, M. Sláma, J. Hodek, L. Ulrychová, J. Weber and K. Obrová, *PeerJ*, 2020, **8**, 10259–10278.
10 J. Feng, *Mater. Lett.*, 2017, **189**, 180–183.
11 F. Zhu, J. Su, Y. Zhao, M. Hussain, S. Yasin, B. Yu and J. Han, *Text. Res. J.*, 2019, **89**, 4173–4185.
12 Y. Huang, H. Brünig, R. Boldt, M. T. Müller and S. Wießner, *Eur. Polym. J.*, 2022, **162**, 110895–110903.
13 C. Yang, X. Jiang, X. Gao, H. Wang, L. Li, N. Hussain, J. Xie, Z. Cheng, Z. Li, J. Yan, M. Zhong, L. Zhao and H. Wu, *Nano Lett.*, 2022, **22**, 7212–7219.
14 X. Xia, X. Shi, W. Liu, S. He, C. Zhu and H. Liu, *Iran. Polym. J.*, 2020, **29**, 581–590.

15 C. Vasile, D. Pamfil, T. Zaharescu, R. P. Dumitriu, G. M. Pricope, M. Râpă and G. Vasilievici, *Polymers*, 2022, **14**, 1398–1426.
16 M. A. Elsawy, M. Fekry, A. M. Sayed, N. A. Maziad and G. R. Saad, *J. Polym. Environ.*, 2022, **10**, 1–21.
17 D. Milicevic, S. Trifunovic, J. Dojcilovic, N. Ignjatovic and E. Suljovrujic, *Nucl. Instrum. Methods Phys. Res., Sect. B*, 2010, **268**, 2744–2749.
18 M. Rzepna, J. Sadło, G. Przybytniak and A. Iuliano, *J. Appl. Polym. Sci.*, 2021, **138**, 50184–50195.
19 J. Zhang, G. Chen, G. S. Bhat, H. Azari and H. Pen, *J. Appl. Polym. Sci.*, 2020, **137**, 48309–48315.
20 H. Zhang, J. Liu, X. Zhang, C. Huang and X. Jin, *RSC Adv.*, 2018, **8**, 7932–7941.
21 X. Li, N. Wang, G. Fan, J. Yu, J. Gao, G. Sun and B. Ding, *J. Colloid Interface Sci.*, 2015, **439**, 12–20.
22 Q. Zhang, F. Liu, T. Y. Yang, X. L. Si, G. R. Hu and C. T. Chang, *Aerosol Air Qual. Res.*, 2017, **17**, 1909–1916.
23 B. Y. Yeom, E. Shim and B. Pourdeyhimi, *Macromol. Res.*, 2010, **18**, 884–890.
24 C. Cai, G. Y. Tang, G. L. Song, L. Zhao and L. j. Chen, *Fuhe Cailiao Xuebao*, 2017, **34**, 486–493.
25 X. Ding, Y. Li, Y. Si, X. Yin, J. Yu and B. Ding, *Compos. Commun.*, 2019, **13**, 57–62.
26 B. C. Shiu, Y. Zhang, Q. Yuan, J. H. Lin, C. W. Lou and Y. Li, *Polymers*, 2021, **13**, 1–13.
27 H. Du, S. Huang and J. Wang, *Sci. Total Environ.*, 2022, **815**, 152980–152988.
28 J. Lee, J. Bae, D. Y. Youn, J. Ahn, W. T. Hwang, H. Bae, P. K. Bae and I. D. Kim, *Chem. Eng. J.*, 2022, **444**, 136460.
29 X.-Y. Gu, L.-M. Hu, Z.-A. Fu, H.-T. Wang and Y.-J. Li, *Chin. J. Polym. Sci.*, 2021, **39**, 1645–1656.
30 R. Ridwan, T. Rihayat, S. Suryani, A. S. Ismi, N. Nurhanifa and S. Riskina, *IOP Conf. Ser.: Mater. Sci. Eng.*, 2020, **830**, 1–7.
31 R. Balen, W. V. da Costa, J. de Lara Andrade, J. F. Piai, E. C. Muniz, M. V. Companhoni, T. U. Nakamura, S. M. Lima, L. H. da Cunha Andrade and P. R. S. Bittencourt, *Appl. Surf. Sci.*, 2016, **385**, 257–267.
32 R. Zhang, W. Lan, T. Ji, D. E. Sameen, S. Ahmed, W. Qin and Y. Liu, *LWT*, 2021, **135**, 110072–110103.
33 A. Marra, C. Silvestre, D. Duraccio and S. Cimmino, *Int. J. Biol. Macromol.*, 2016, **88**, 254–262.
34 A. M. A. El Sayed and N. A. El Sayed, *Arabian J. Geosci.*, 2021, **14**, 1–11.
35 Z. Chen, W. Zhang, H. Yang, K. Min, J. Jiang, D. Lu, X. Huang, G. Qu, Q. Liu and G. Jiang, *Environ. Sci.: Processes Impacts*, 2022, **24**, 649–674.
36 A. Alsabbagh, R. Abu Saleem, R. Almasri, S. Aljarrah and S. Awad, *Polym. Bull.*, 2021, **78**, 4931–4945.
37 P. Benyathiar, S. E. Selke, B. R. Harte and D. K. Mishra, *J. Polym. Environ.*, 2021, **29**, 460–471.
38 M. Peng, H. Jia, L. Jiang, Y. Zhou and J. Ma, *J. Text. Inst.*, 2018, **110**, 468–475.
39 J. Bao, X. Dong, S. Chen, W. Lu, X. Zhang and W. Chen, *J. Polym. Sci.*, 2020, **58**, 455–465.
40 P. Benyathiar, S. E. Selke, B. R. Harte and D. K. Mishra, *J. Polym. Environ.*, 2020, **29**, 460–471.
41 X. Zhang, J. Liu, H. Zhang, J. Hou, Y. Wang, C. Deng, C. Huang and X. Jin, *Polymers*, 2021, **13**, 1–14.
42 E. Dzierzkowska, A. Scislowska Czarnecka, M. Kudzin, M. Bogun, P. Szatkowski, M. Gajek, K. Kornaus, M. Chadzinska and E. Stodolak Zych, *J. Funct. Biomater.*, 2021, **12**, 1–17.
43 F. Zhu, B. Yu, J. Su and J. Han, *Autex Res. J.*, 2020, **20**, 24–31.
44 J. Yan, K. Dong, Y. Zhang, X. Wang, A. A. Aboalhassan, J. Yu and B. Ding, *Nat. Commun.*, 2019, **10**, 1–9.
45 M. Maiza, M. T. Benaniba, G. Quintard and V. Massardier Nageotte, *Polimeros*, 2015, **25**, 581–590.
46 C. M. Cobos, L. Garzón, J. L. Martinez, O. Fenollar and S. Ferrandiz, *Rapid Prototyp. J.*, 2019, **25**, 738–743.
47 H. Zhang, N. Liu, Q. Zeng, J. Liu, X. Zhang, M. Ge, W. Zhang, S. Li, Y. Fu and Y. Zhang, *Polymers*, 2020, **12**, 2341–2343.
48 F. Zhu, J. Su, M. Wang, M. Hussain, B. Yu and J. Han, *J. Ind. Text.*, 2020, **49**, 748–772.
49 D. Chmielewska, Ł. Werner, U. Gryczka and W. Migdał, *Nukleonika*, 2022, **67**, 23–33.
50 Y. Kara and K. Molnár, *J. Ind. Text.*, 2022, **51**, 137–180.
51 J. Zhang, H. Wang, C. Chen, A. Gui, X. Zhang, Y. Wang, Y. Xiong and W. Zeng, *J. Phys.: Conf. Ser.*, 2022, **2194**, 1–6.
52 K. Xu, L. Zhan, R. Yan, Q. Ke, A. Yin and C. Huang, *Nanoscale*, 2022, **14**, 419–427.
53 P. He, F. Wu, M. Yang, W. Jiao, X. Yin, Y. Si, J. Yu and B. Ding, *Compos. Commun.*, 2021, **25**, 100720–100726.
54 S. Chiera, A. Cristoforetti, L. Benedetti, G. Nollo, L. Borro, L. Mazzei and F. Tessarolo, *Int. J. Environ. Res. Public Health*, 2022, **19**, 3548–3567.